Received: 8 March 2022 | Revised: 19 September 2022 | Accepted: 22 September 2022

DOI: 10.1002/eqe.3755

RESEARCH ARTICLE

WILEY

On the seismic performance of straight integral abutment bridges: From advanced numerical modelling to a practice-oriented analysis method

Andrea Marchi[1] | **Domenico Gallese**[2] | **Davide Noè Gorini**[1] | **Paolo Franchin**[1] | **Luigi Callisto**[1]

[1]Department of Structural and Geotechnical Engineering, Sapienza University of Rome, Rome, Italy (Email: andrea.marchi@uniroma1.it)

[2]Ove Arup & Partners International Ltd., London, UK

Correspondence
Paolo Franchin, Department of Structural and Geotechnical Engineering, Sapienza University of Rome, Via Antonio Gramsci 53, 00197 Rome, Italy. Email: paolo.franchin@uniroma1.it

[Correction added on 5 December 2022, after first online publication: CRUI funding statement has been added.]

Funding information
Universita degli Studi di Roma La Sapienza

Abstract

The seismic performance of integral abutment bridges (IABs) is affected by the interaction with the surrounding soil, and specifically by the development of interaction forces in the embankment-abutment and soil-piles systems. In principle, these effects could be evaluated by means of highly demanding numerical computations that, however, can be carried out only for detailed studies of specific cases. By contrast, a low-demanding analysis method is needed for a design-oriented assessment of the longitudinal seismic performance of IABs. To this purpose, the present paper describes a design technique in which the frequency- and amplitude-dependency of the soil-structure interaction is modelled in a simplified manner. Specifically, the method consists of a time-domain analysis of a simplified soil-bridge model, in which soil-structure interaction is simulated by means of distributed nonlinear springs connecting a free-field ground response analysis model to the structural system. The results of this simplified method are validated against the results of advanced numerical analyses, considering different seismic scenarios. In its present state of development, the proposed simplified nonlinear model can be used for an efficient evaluation of the longitudinal response of straight IABs and can constitute a starting point for a prospective generalisation to three-dimensional response.

KEYWORDS
construction stages, nonlinear dynamic analysis, OpenSees, seismic design method, soil-structure interaction, Winkler

1 | INTRODUCTION

Integral abutment bridges (IABs), characterised by a monolithic connection (full transmission of forces and moments) of the deck with the abutments, are being increasingly employed all over the world. This bridge type is characterised by lower construction and maintenance costs if compared to traditional structural schemes, due to the absence of bearings and deck joints that in turn results in significant advantages in the maintenance and inspection plans. The use of IABs

is encouraged by recent studies demonstrating that several such bridges subjected to strong ground motion in California and New Zealand showed a better performance than conventional construction types.[1,2]

The country with the largest number of IABs is by far the USA, with tens of thousands of structures built from the 1930s to date.[3] Since the 1950s, this structural typology has been largely employed also in Europe,[4–7] where the construction practices differed somewhat from those adopted in the USA.[8,9] More recently, IABs have been realized in many other countries, e.g. in Japan,[10,11] and Australia.[12]

Despite the large experience gained worldwide, the design of IABs is still affected by several uncertainties, which are mainly related to the assessment of the effects induced by the soil on the structural members, under both static and dynamic conditions. Several research studies focused on the evaluation of the soil-structure contact pressures exchanged along the abutment front wall accounting for the cyclic thermal deformations in the deck.[13–17] Thermal expansion may produce important interaction forces in the abutments and at their connection with the deck, depending on the deformability of the soil-abutment system, that may limit the use of an integral abutment-deck connection to short- and medium-span bridges.[18,19] This drawback can be overcome by designing a deformable abutment, supported by a single pile row, capable to accommodate the thermal deformation of the deck,[20] and in fact, design recommendations to this effect were published by the UK Highways Agency in its publication BA42/96[21] and in its Amendment No. 1.[22] Alternative measures to control the contact pressure at the soil-abutment contact include the use of pressure-relief joints and cycle-control joints between the approach slabs and the approach pavements[23] and the use of specific construction sequences.[4]

The measurements provided by Werner et al.[24] on two highway overcrossings located in California (Painter Street Overcrossing and the Meloland Road Overcrossing) during strong motion were taken as the reference for many numerical studies.[24–36] All these studies, as well as other advanced numerical investigations carried out by Elgamal et al.,[37] Gorini and Callisto[38] and Gorini et al.[39] on different soil-bridge layouts pointed out the central role played by the approach embankments on the overall dynamic response. Simplified analytical and numerical models[32,40–42] have been proposed through the years for a direct consideration in the seismic design of bridges of the frequency-dependent inertial forces developing in the embankments. Nonetheless, the structural continuity between deck, abutment and foundation piles seems to require a full consideration of the soil-pile interaction in the seismic design of IABs.

As already pointed out, there is still a lack of reliable design rules and guidelines for the seismic design of IABs. For this reason, this typology was explicitly included in the mandates of the Eurocode Committee for the evolution of Eurocodes by 2020. To date, a well-established option is to describe the soil-bridge interaction through nonlinear Winkler-type models. The earliest application of the approach appeared in Greimann et al.,[43] where it was used in both bi- and three-dimensional analyses: the Winkler springs were nonlinear, and the study focussed on temperature induced cycles, rather than on the seismic response. Later, Faraji et al.[44] showed that this class of models can be easily implemented into commercial finite element software, demonstrating the practical importance of this approach. Once again, as in most earlier applications, the focus was therein on the stresses and deformation induced by the thermal excursions of the deck. A Winkler-type model was also adopted in Dicleli and Erhan[45] to investigate the effect of soil stiffness on the structural internal stresses under traffic loads, and by Dicleli and Erhan[46] to investigate eventually the seismic performance. Along similar lines, and following their previous work on the seismic analysis of flexible earth-retaining diaphragm walls,[47] Franchin and Pinto[48] modelled the soil in the free-field as a one-dimensional shear beam with variable cross-section. Likewise, one-dimensional frame elements were used for the structure, while the soil-structure interaction was simulated through nonlinear Winkler springs.

Within this context, the present paper generalises the simplified methodology proposed by Franchin and Pinto[48] for a more realistic consideration of the dynamic soil-structure interaction effects occurring at the abutment locations. As a term of comparison, a large numerical model of the soil-bridge system is considered, to test the predictive capability of the proposed method for different seismic scenarios. A detailed reproduction of the construction sequence is introduced in the proposed approach, and its influence on the bridge performance is critically assessed. Through a systematic comparison between the refined and the reduced-order models, a rational calibration for the input parameters of the latter is devised, with specific reference to the identification of the mass, stiffness and strength properties of the soil interacting with the abutment.

2 | CASE STUDY

2.1 | Structural and soil properties

The case study examined in this paper is inspired by an integral overpass recently built in Italy along the A14 Adriatic highway, named Gatteo highway overpass.[4] Figure 1 shows the bridge layout: it is composed of a single span, supported

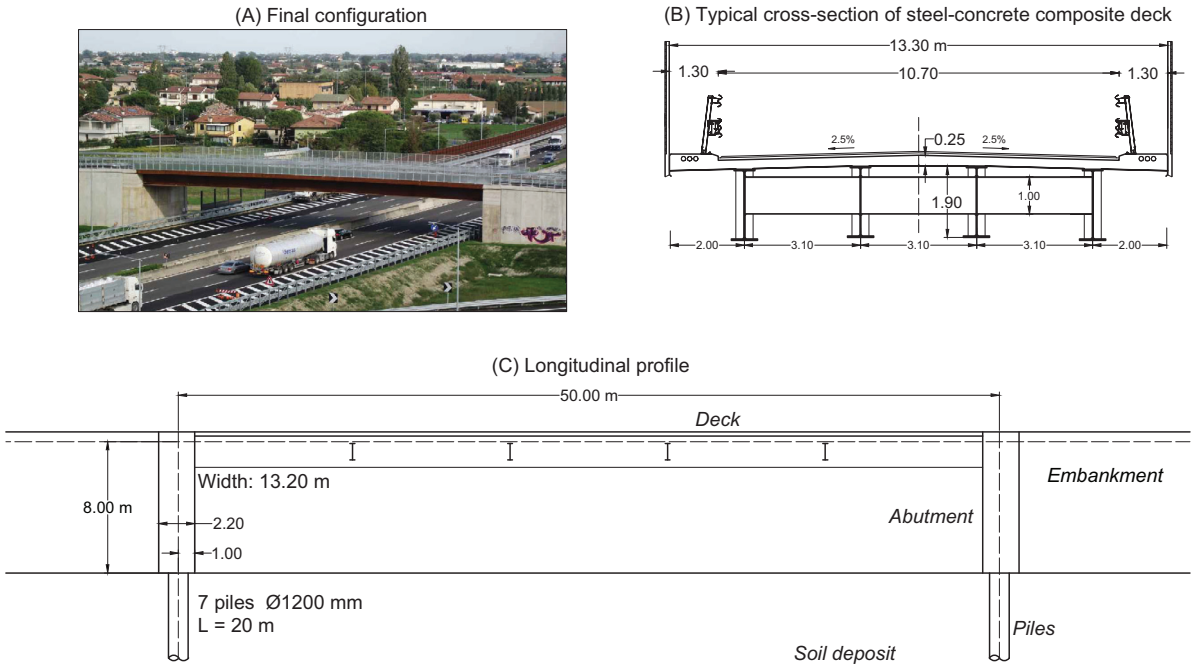

FIGURE 1 (A) view of the Gatteo highway overpass in service[4]; (B) cross-section of the steel-concrete composite deck of the bridge; (C) longitudinal profile of the structural layout.

TABLE 1 Deck elastic properties

Cross-section	EA (MN)	EI (MN m^2)	m (Mg)
steel only	6.2×10^4	1.0×10^5	225.3
composite	2.5×10^5	1.4×10^5	956.4

TABLE 2 Soil properties

Soil domain	ρ_s (Mg/m^3)	K_0 (-)	φ' (°)
Embankment	2.04	0.43	36
layer 1	2.04	0.46	33
layer 2	2.04	0.43	35

by two integral abutments. The bridge deck has a length of 50.0 m. Its cross-section consists of a steel-concrete composite structure formed by four welded I-shaped plate girders, having a height of 1.9 m, transversally connected by secondary 1.0 m high steel beams and by the concrete slab, the latter having a thickness and width of 0.25 and 13.3 m, respectively. Table 1 summarizes the elastic deck properties, distinguishing the steel section, which is the resisting section in the initial construction stages, from the final composite section. Specifically, E is the Young modulus, I is the second moment of inertia, A is the cross section area, and m is the total mass, including all the non-structural elements of the deck.

The reinforced-concrete 8.0 m high front wall of the abutment has a rectangular cross section with a width of 13.2 m and a thickness of 2.2 m and is supported by a single row of seven reinforced concrete piles, having a length of 20.0 m and a diameter of 1.2 m. The soil deposit includes two dry layers of gravelly sand of increasing stiffness. The properties of the coarse-grained embankment were determined according to the procedure proposed by Gorini[49] to comply with the Italian technical provisions on the grain size distribution, stiffness and strength of embankments.[50] Figure 2 shows the profile of the small-strain shear modulus G_0, in which the dashed line considers the increase in effective stresses produced by the embankment. Table 2 reports the relevant soil properties for this study, namely the mass density ρ_s, the earth pressure coefficient at rest K_0, and the angle of shearing resistance φ'.

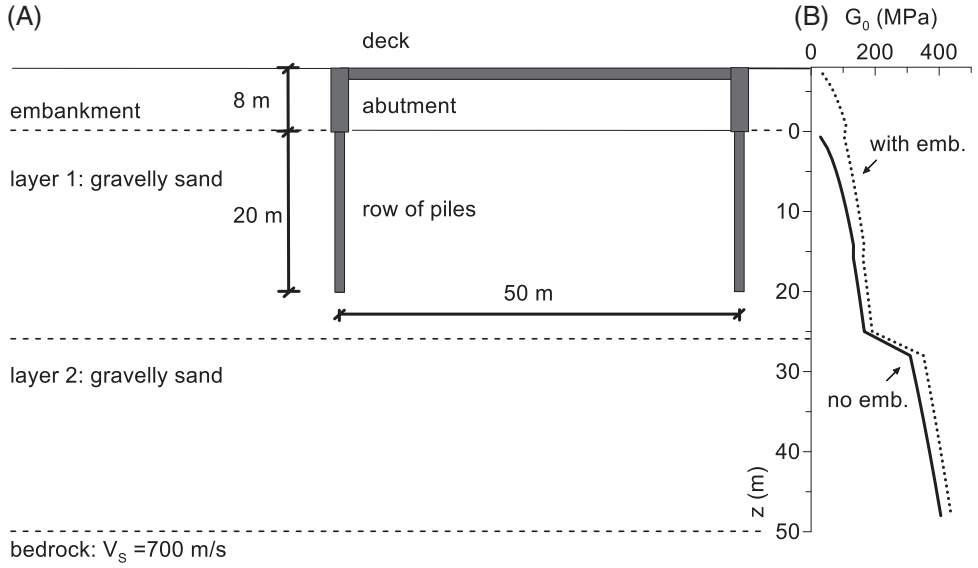

FIGURE 2 (A) schematic representation of the reference soil-bridge layout; (B) profile of the small strain shear modulus, G_0, with depth.

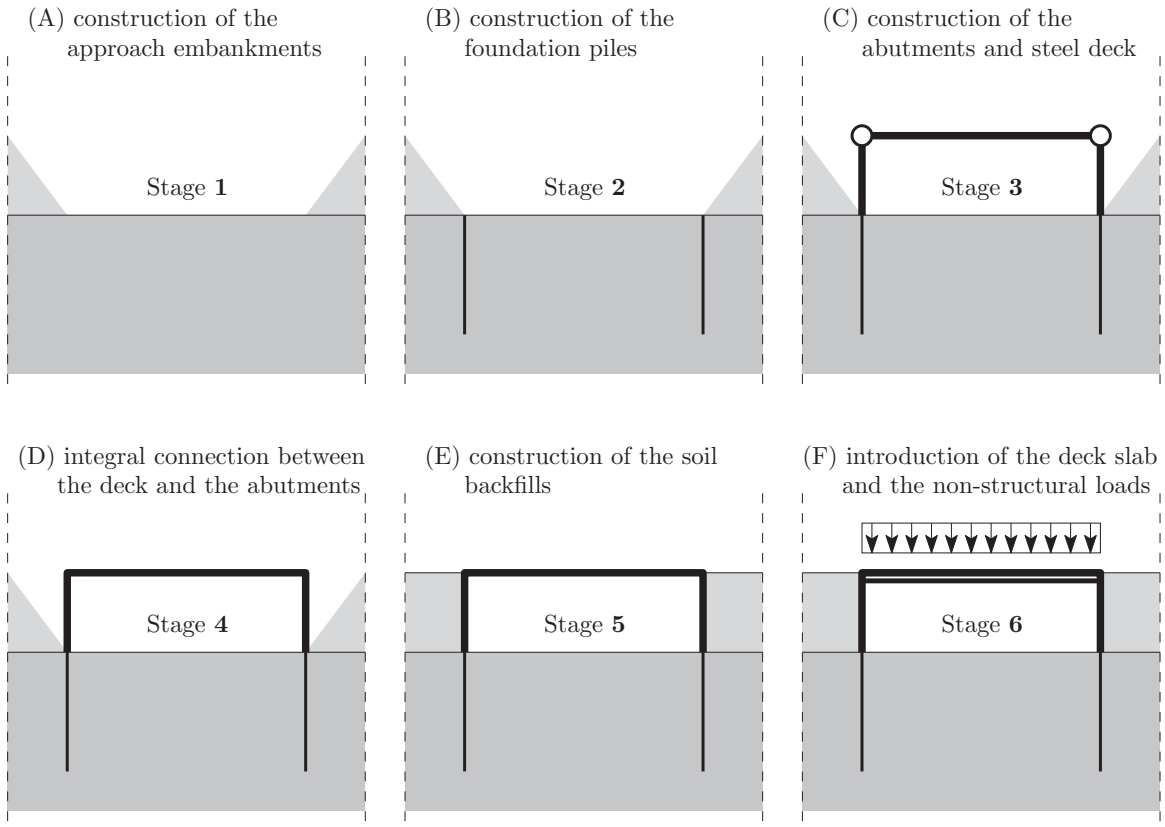

FIGURE 3 Construction sequence for the reference integral abutment bridge.

2.2 | Construction stages

The construction sequence of the bridge considered herein is depicted in Figure 3 reproducing closely that actual sequence employed in the construction of the prototype bridge: it is aimed at minimising the internal forces in the deck and in the foundation piles under the service loads. Starting from the lithostatic conditions of the foundation soils, the two sides of the approach embankment are built first, to avoid deflection and down-drag of the foundation piles. Subsequently the

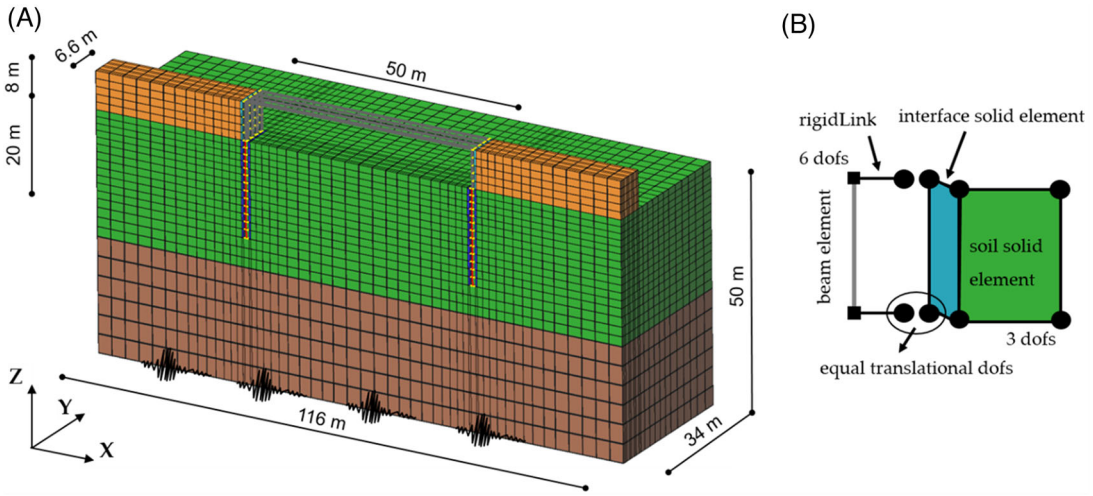

FIGURE 4 (A) 3D model of the soil-bridge system developed in OpenSees, and (B) detail of the connection between beam and solid elements .

piles, the abutments and the deck are constructed, keeping the embankment away from the front walls. In the present stage (No.3 in the figure) the deck is simply supported at the abutments through a hinged connection and includes only the steel girders and the secondary beams. The integral connection of the deck to the abutments follows (Stage No. 4) and the soil fill is placed behind the front walls bringing the embankment in contact with the abutments (Stage No. 5). Finally, in Stage No. 6, the concrete slab is cast-in-place and the non-structural loads are applied to the deck.

Finally, it should be noted that the approach slab, built in Stage 5, is not shown. These slabs are designed to ensure a smooth transition between the bridge deck and the embankment and to avoid damage to the road surface. The practice presents regional differences, in terms of slab length, its inclination, depth and detail of connection with the abutment, see, for example, Thiagarajan et al.[51] and Dreier at al.[52] By changing the amount of soil involved in the abutment wall displacement, the slab has the potential of influencing the overall response. This was investigated with a separate parametric study (not shown), carried out within the analysis software Optum.[53] It was shown that for the typical parameters of the Italian/European practice (length lower/equal to 1.2 times the extension of the active soil wedge behind the abutment, inclination lower/equal to 10° from the horizontal and burying depth lower than 20% of the abutment height), the approach slab has limited influence on the bridge response. In the following, it is therefore neglected both in the refined and in the reduced order model.

3 | NUMERICAL MODELS

3.1 | Three-dimensional finite element model

A three-dimensional (3D) finite element model of the reference soil-bridge system was developed using the analysis framework OpenSees.[54] The main features of the 3D model are illustrated in the following, while the reader can refer to Gallese[55] and Gallese et al.[56] for a more comprehensive description of the implementation.

The finite element mesh, shown in Figure 4, includes the deck, the abutments, the piled foundations and the soil domain. Since the analyses focus on the longitudinal response, only half of the bridge was modelled, taking advantage of the symmetry of the problem about the vertical longitudinal plane. The extension of the model in both the longitudinal (x) and transverse (y) directions, indicated in Figure 4, was chosen after a parametric study to minimise the effect of spuriously reflected waves, while keeping the overall size of the model within manageable limits.

The soil domain of Figure 4 includes about 26,000 eight-node brick elements with physically stabilized single-point integration (*SSPbrick*-class finite element[57] in the OpenSees library). For simplicity, an equivalent rectangular cross-section was assumed for the embankments: to avoid local instability of the lateral sides of the embankment, equal transverse displacements of corresponding lateral nodes were enforced. This modelling strategy simulates in practice an embankment made of reinforced earth. The structure, formed by the piles, the abutments and the deck, was modelled with about 700

two-nodded beam elements exhibiting a linearly elastic behaviour. A grillage modelling approach was adopted for the abutment walls and the deck, with the properties of each beam taken proportional to its area of influence.

To connect the piles to the surrounding soil, the solid elements in the region occupied by the piles were removed, and at each elevation the pile nodes were connected to the corresponding soil nodes using rigid-body constraints (*RigidLink* kinematic constraint in the OpenSees library). In addition, thin layers of solid elements with reduced strength properties (soil-wall friction $\delta = 2/3\ \varphi$') were added along the pile shaft to model the soil-pile interface (Figure 4.B). The same procedure was applied to connect the abutment elements to the corresponding embankment elements.

The mechanical behaviour of the soil was simulated using the elastic-plastic model proposed by Yang et al.[58] This is a pressure-dependent, multi-yield model with kinematic hardening and non-associated plastic flow (*PDMY* in the OpenSees library). Its calibration for the case at hand was exhaustively discussed by Gallese.[55]

After the simulation of the construction stages, time-domain dynamic analyses were carried out on the 3D model, applying the seismic motion to its base through viscous dampers to simulate the presence of a compliant bedrock.[59] Because the structural members of the bridge were designed to exhibit an elastic behaviour under strong ground motion (see also Section 3.2), the main source of energy dissipation is represented by the plastic strains occurring in the soil. Nevertheless, a small viscous damping ratio not greater than 2 % in the range of the significant modal frequencies of the bridge (see Section 4.1) was assigned to the full soil-structure domain using the Rayleigh formulation to reproduce energy dissipation at small strain levels and attenuate the effects of spurious high frequencies.

With the aim of speeding up the calculation time, the OpenSees parallel computing was employed by using the application OpenSeesSP.[60] The system solver Multifrontal Massively Parallel sparse direct Solver (MUMPS) was adopted to solve the large sparse system of equations. A Newmark time-stepping method with $\gamma = 0.5$ and $\beta = 0.25$ was used to integrate the equation of motion, while the Newton-Raphson algorithm was employed to solve the nonlinear residual equation.

3.2 | Reduced-order model

Because of the complex modelling and the relevant computational demand, the 3D model described above cannot be regarded as an efficient design tool. In the present work this complex model was used as a benchmark to assess the validity of a simpler, design-oriented model, referred to herein as Reduced-Order Model (ROM), developed in Marchi,[61] as an extension of the model initially proposed by Franchin and Pinto.[48] The ROM models consider in a simplified manner the soil domain: specifically, the interaction between the structural members and the soil is described by means of mutually independent, nonlinear uniaxial springs.

Two implementations of the ROM were developed in two different computing environments, namely the commercial finite element software Sap2000[62] and the open-source finite element analysis framework OpenSees.[54] In the following, the differences in the two numerical models, denoted as ROM-S2K and ROM-OS, respectively, are commented, with a particular focus on soil-structure interaction.

Figure 5 illustrates the conceptual scheme of the ROM: it is conceived to determine the longitudinal response of straight IABs through response-history analysis. The structure is in contact with the soil surrounding the foundation piles and with the embankments through horizontal, nonlinear springs that are called upon to reproduce the effects of the soil-structure interaction. On each side of the bridge the foundation soils and the embankment are modelled as one-dimensional soil-embankment shear columns simulating the seismic ground response in the free-field (the figure shows only half of the model due to symmetry in the case study).

The structural components of the bridge can be modelled using different strategies. In the original proposal by Franchin and Pinto,[48] the deck was modelled with a single line of beam elements at the deck centroid or at the top central fibre, with the full inertial properties of the composite steel-concrete section assigned to the deck elements from the beginning. By contrast, in this work all the construction stages described in Section 2.2 were fully considered. In Sap2000 this was done using the nonlinear staged construction option, while in OpenSees the *UpdateParameter* command was used to modify specific element properties. A simple linear elastic behaviour was assigned to the structural elements, for consistency with the 3D model. The choice of elastic behaviour for these components is consistent with the intended performance under the design seismic action, according to the draft of the European regulations on the design of such bridges.[63] Note that inclusion of inelastic behaviour for the structural members in both the refined and the reduced-order model is possible, and when both are implemented in the OpenSees platform, it can be done with exactly the same formulation.

Nonlinear compression-only Winkler springs (two-noded elements of type *TwoNodeLink* in OpenSees and *NLLink* in Sap2000) simulate the mobilisation of the active and passive limit states in the soil through a piecewise linear relationship

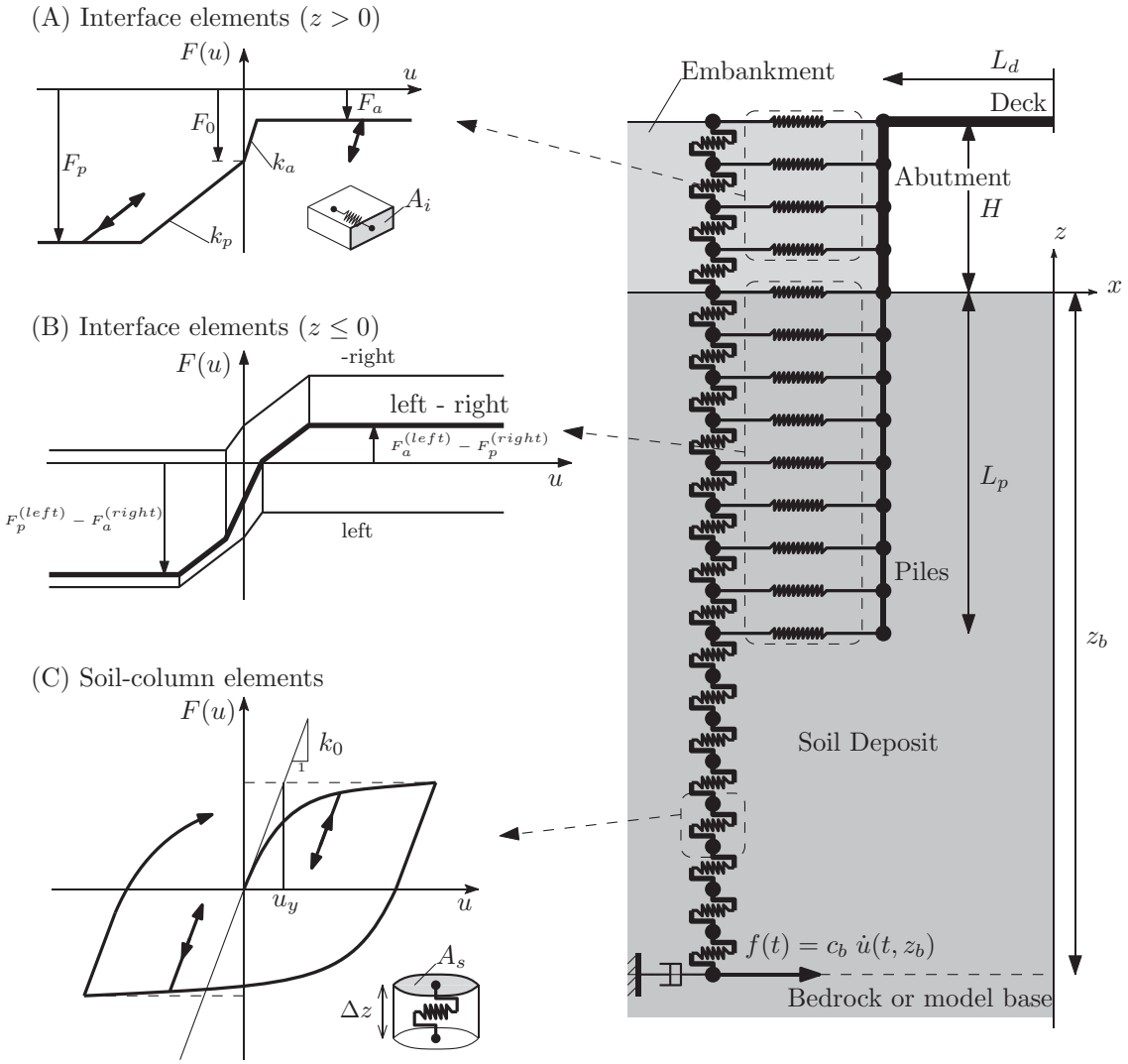

FIGURE 5 Layout of the reduced-order model and (C) representation of the constitutive laws assigned to the foundation soil and embankment elements, and (A,B) soil-structure interfaces.

between the spring forces and displacements (Figure 5A). The soil resistance is expressed as a function of the vertical effective stress through the active and passive earth pressure coefficients K_A and K_P, that depend on the angle of shearing resistance of the soil and on the soil-wall friction according to the lower-bound solution proposed by Lancellotta.[64] The angle of soil-wall friction δ was taken equal to $2/3\ \varphi'$ for consistency with the interface behaviour of the 3D model, while the effect of the seismic intensity variation on the earth pressure coefficients was neglected, as this would have implied values of K_A and K_P variable in time: a single seismic coefficient value k_h, was used to determine K_A and K_P in each analysis, corresponding to the peak ground acceleration of the seismic input. A major issue is the need to pre-load the springs to reproduce the earth pressure at rest. While this can be easily simulated in OpenSees (either by coding a uniaxial multi-linear plastic compression-only law or using the Parallel command with existing uniaxial laws), Sap2000, to date, does not allow non-centred constitutive laws (null displacement may not correspond to a non-zero force). For this reason, in the ROM-S2K the at-rest contact forces were applied as external forces to the abutment, while the yield forces of the springs were taken as proportional to reduced earth pressure coefficients $\tilde{K}_A = K_A - K_o$ and $\tilde{K}_P = K_P - K_o$, where K_o is the earth pressure coefficient at rest. The stiffness coefficients k_a and k_p (see Figure 5a) were related to the Young's modulus as reported by Pinto and Franchin[48] converting the distribution of the small-strain shear modulus of Figure 2B into an equivalent variation of the Young's modulus, using a Poisson's coefficient of 0.3.

A single compression-only spring can be used to model the interaction above z = 0, where the abutment wall is characterized by single-sided contact. For the foundation piles, on the other hand, the soil-pile contact is bilateral and one can

TABLE 3 Summary of model parameters' values for the ROM; minimum and maximum values are given for parameters that are depth-dependent

	Parameter	Units	Value	min	max
Soil deposit	L_e	m	44	–	–
	B_s	m	13.2	–	–
	c_b	Mg/s	1.6×10^6	–	–
	k_0	kN/m	–	3×10^7	4×10^8
	F_y	MN	–	7.8	1613
	m	Mg	–	947	1857
Interfaces	K_0	–	–	0.41	0.46
	K_A	–	–	0.26	0.29
	K_P	–	–	4.78	6.00
	k_a	MN/m	–	217	1245
	k_p	MN/m	–	113	734

either use a pair of opposite springs, so that their compression forces act against the pile from both sides, or a single spring with the resultant force-displacement relationship. Figure 5B shows the latter option, where it can be observed how, due to the different average effective stresses caused by the embankment, the properties of the two springs are not the same and the force-displacement law resulting from their sum is not symmetric. Finally, it is noted that springs also follow the construction stages and, for example, the interface elements on the abutment wall (z > 0) are activated only in Stage 5 (together with K_0 forces, in Sap2000).

The shear-type soil-embankment columns are composed of two-noded elements (*TwoNodeLink* in OpenSees and *NLLink* in Sap2000) with a uniaxial Bouc-Wen force-displacement law[65,66] aimed at describing the soil response far from the structure (Figure 5C). The use of the Bouc-Wen model to describe the shear behaviour of soil in the context of site response analysis is documented, for example, in Gerolymos and Gazetas,[67] Drosos et al.[68] In particular, in the latter work the authors provide values of a modified Bouc-Wen model calibrated to reproduce the response of soils categorized in terms of effective confining stress and plasticity index according to the model of Ishibashi and Zhang.[69] The modified Bouc-Wen law provided in Gerolymos and Gazetas[67] to better describe fine features of the cyclic behaviour of soils was implemented in the present work in OpenSees. In Sap2000, instead, a more basic version of the Bouc-Wen constitutive law was used in which, for instance, the parameters controlling the shape and size of the hysteresis loop under cyclic loading, denoted as β and γ in Gerolymos and Gazetas,[67] cannot be differentiated as instead proposed by Drosos et al.[68]

To complete the calibration of the soil-embankment column, forces in the Bouc-Wen model should be related to the shear stresses in the soil, and the masses connected to the springs should be related to the soil density, as follows:

$$F = \tau A_e \quad M = \rho \Delta z A_e$$

where Δz is the distance between the column element nodes, and A_e is an equivalent transverse area of the soil (see Figure 5). To enforce a free-field response of the soil column, this area was set to be sufficiently larger to make the dynamic response of the system independent from its choice. This was obtained with an area A_e corresponding to a mass M equal to about 200 times that of the single abutment structure.

Viscous dampers were applied to the base of the soil columns to simulate a compliant bedrock, with a damping coefficient c_b equal to $\rho_b V_b\ A_e$, where $\rho_b = 2.5\ Mg/m^3$ and $V_b = 700\ m/s$ are the density and the shear wave velocity of the bedrock, respectively. Following Joyner and Chen[59] and consistently with the 3D model, the seismic input was applied as a time history of shear forces (see Figure 5):

$$f(t) = c_b \dot{u}_b(t)$$

where $\dot{u}_b(t)$ is the velocity time-series of the seismic motion at the outcrop.

In conclusion, a total of 294 linear or non-linear elements (120 beam elements, 110 uniaxial Bouc-Wen elements, 62 uniaxial Winkler elements, and two uniaxial dashpots) were employed to describe the problem with the ROM. Table 3

TABLE 4 Significant vibration modes of the bridge, computed with the 3D model, the ROM, and the 1D soil column (the symbol * indicates vertical modes)

3D model			ROM			1D soil column		
Mode No.	T_i (s)	M_{SSI} (%)	Mode No.	T_i (s)	M_{SSI} (%)	Mode No.	T_i (s)	M_{SSI} (%)
1	0.62	70.8	1	0.60	70.2	1	0.63	72.9
–	–	–	2*	0.30	25.5	–	–	–
4	0.27	13.1	3	0.24	12.9	2	0.24	15.3
7	0.16	1.9	4	0.17	4.0	3	0.15	5.3

summarizes the values of the ROM parameters adopted for the case study, while a scheme that links the input data required to set the ROM with its parameters is provided in the appendix at the end of the paper.

4 | VALIDATION OF THE REDUCED-ORDER MODEL

Taking the response of the 3D model as a term of comparison, the proposed ROM is validated in terms of the modal characteristics of the entire soil-structure system (Section 4.1), internal forces due to construction stages (Section 4.2), amplification of ground motion through the soil domain (Section 4.4) and, finally, seismic response under two different ground motion scenarios (Section 4.5).

4.1 | Modal properties of the soil-bridge system

A modal analysis of the reference soil-bridge system was carried out using the 3D model and the ROM. Note that the modal response of both implementations of the ROM are practically coincident. The effective variability of the small-strain elastic stiffness of the soil with the stress state at the end of the construction sequence was considered implementing the procedure developed by Gallese et al.[56]

The comparison between the 3D model and the ROM is restricted to the first three longitudinal modes. The modal vibration periods, T_i, and effective masses, M_{SSI}, are reported in Table 4 together with the response of the free-field soil column (including the embankment), while the corresponding modal shapes are depicted in Figure 6. For all the models the first longitudinal mode occurs at a period of about 0.62 s, very close to the first mode of the free-field soil column. In this mode, the structure follows the displacements impressed by the surrounding soil, with an overall translation and inflection of the abutments.

The higher-order modes are directly related to the dynamic participation of the deck in the vertical direction (mode no. 2 in the ROM) and of the embankments (modes no. 3 and 4 in the ROM). In particular, these latter modes represent the first and second modes of the approach embankments in the longitudinal direction, whose modal properties are nearly coincident to the ones obtained with the 3D model. As it was demonstrated in recent and less recent studies,[38,39,48] the embankment modes strongly affect the structural performance because they are related to the flexural behaviour of the abutments (see Figure 6).

Therefore, it would seem that the dynamic response of the system is primarily controlled by the soil, because of the very large mass interacting with the structure, whose effects are transferred to the entire structural layout as a consequence of the integral deck-abutments connection. This is also confirmed by the vibration modes of the free-field soil column (Table 4 and Figure 6), that are quite similar to the corresponding modes of the soil-structure system. As the modal shapes of Figure 6 indicate significant curvatures at the deck-abutment contact and at the piles head, it is evident that the internal forces computed at these locations deserve a special attention.

4.2 | Construction stages

In both the 3D model and the ROM, a staged analysis procedure was adopted to simulate the initial state in the soil-structure system at the end of the bridge construction, as a crucial aspect for a realistic evaluation of the subsequent

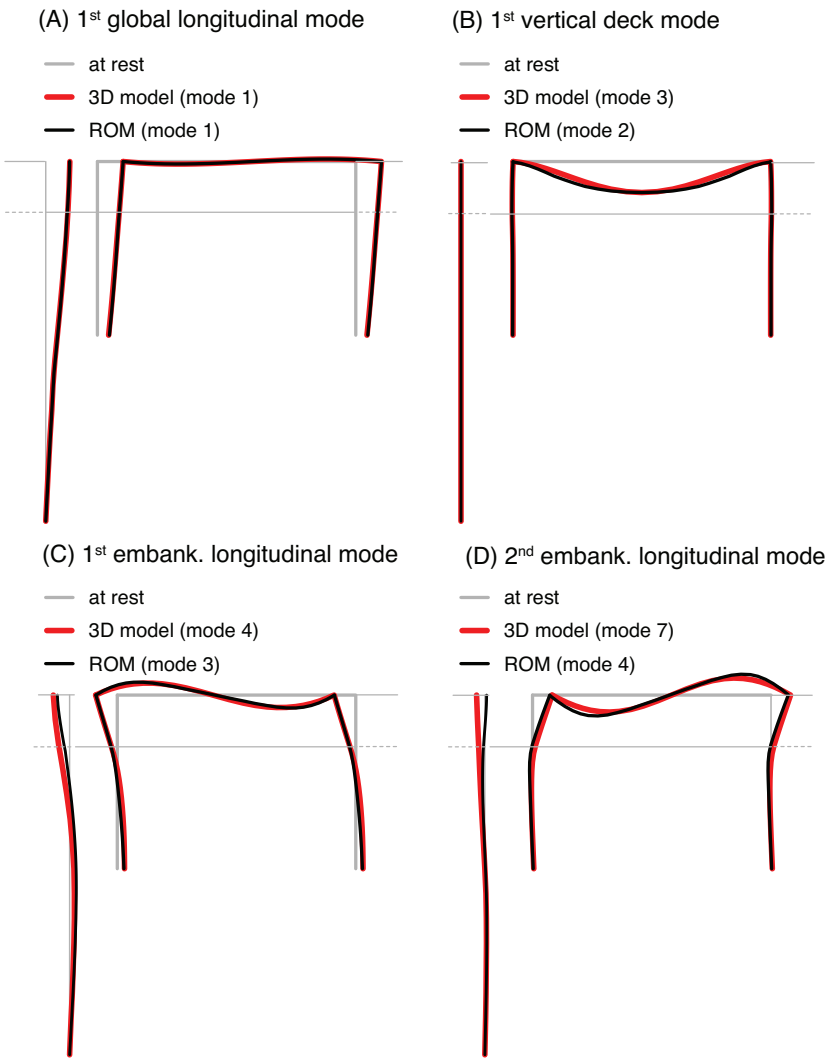

FIGURE 6 Significant modal shapes of the reference bridge obtained with the 3D model and the ROM.

seismic response. The construction sequence described in Section 2.2 was implemented in OpenSees and Sap2000. The reader can refer to Gallese et al.[39] for a detailed description of the strategy used in the 3D model. As per the ROM, as already said, in OpenSees the construction stages are implemented in the model by means of elements whose parameters are progressively updated (e.g. in Stage No. 3 a rotational spring of negligible stiffness is introduced in the relative rotation degree of freedom of deck and abutment, and in Stage No. 4 the stiffness is increased to a sufficiently large value to simulate fixity), while in Sap2000 a *Nonlinear Staged Construction* load case is used.

Figure 7 shows the horizontal displacements and the distribution of bending moments in the piles and in the front wall for the last two construction stages of Figure 3, that is the completion of the backfill behind the front wall (stage No. 5) and of the composite structure of the deck (stage No. 6). The results of the full 3D model and the ROM are almost coincident for both stages. Stage No. 5 causes a deformation of the abutment away from the embankment, maximising the bending moment at the top of the piles. Completion of the deck structure (stage No. 6) reverses the abutment displacement, reducing the bending moment at the top of the pile but producing significant internal forces at the deck-abutment connection. Therefore, the analysis of the construction stages confirms the indication of the modal analysis that the deck-abutment connection and the pile top sections are the crucial components of the structural system.

4.3 | Seismic input

Two ground motion time-series, referred to in the following as Parkfield and Yamakoshi, were selected from the PEER ground motion database (https://ngawest2.berkeley.edu/) to test the response of the ROM to different motion amplitudes

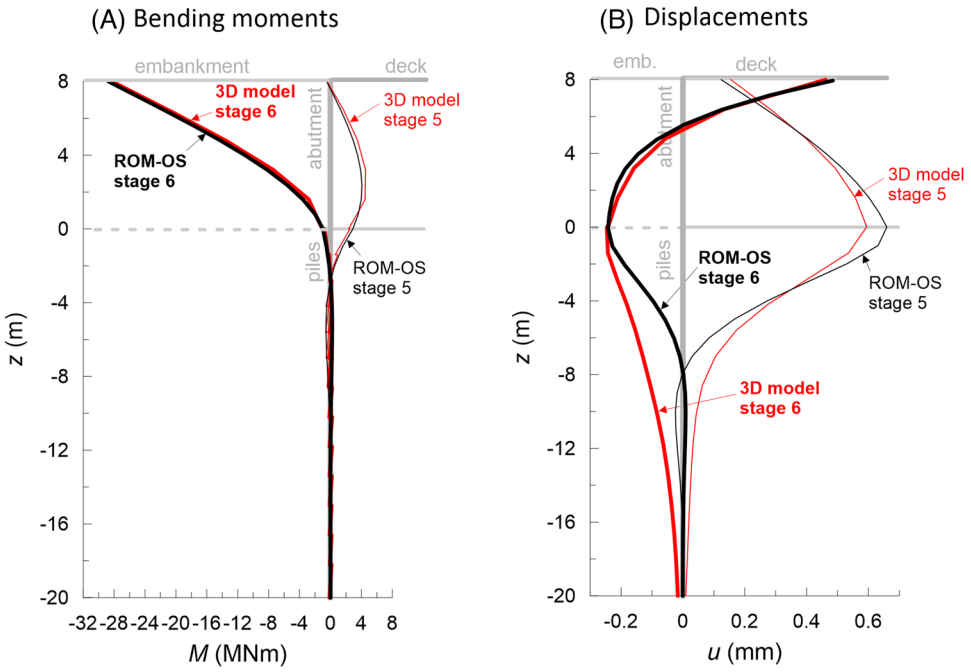

FIGURE 7 (A) Profiles of the bending moment and (B) the horizontal displacements in the left piles and abutment front wall relative to the construction stages no. 5 and 6.

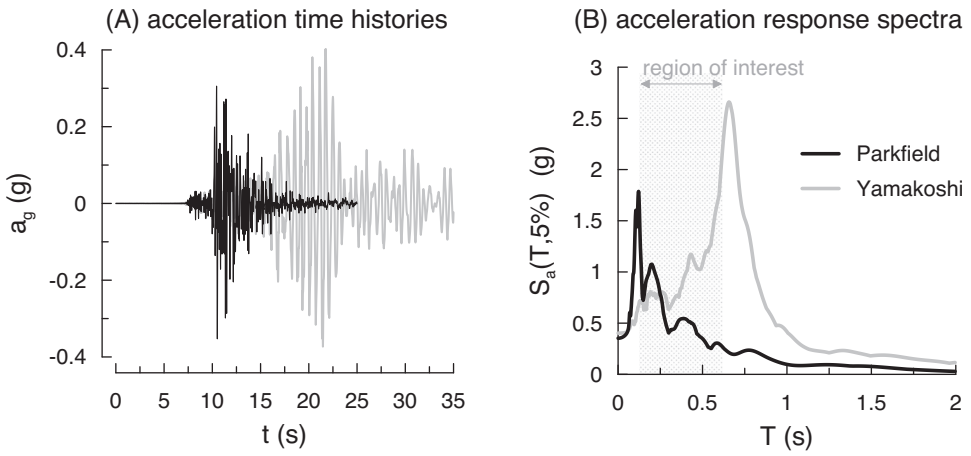

FIGURE 8 (A) Acceleration time histories and (B) 5%-damped elastic response spectra of the two selected seismic records, with representation of the spectral region of interest for the dynamic response of the bridge derived from the modal analysis.

and frequency contents. The moment magnitude (M_w = 6.0-6.8) and the Joyner and Boore distance (R_{JB} = 4–23 km) of the two events are compatible with the seismo-tectonic setting at the bridge location.

Figure 8 shows the acceleration time histories and the 5% damped elastic response spectra for the two selected records, which show a complementary spectral response in the period interval 0–1 s: the maximum spectral ordinates for the more severe Yamakoshi record occur in the period range of 0.5–0.8 s, exciting the fundamental global mode of the soil-bridge system (Figure 6A); conversely, for the Parkfield record the maximum spectral accelerations are relative to periods lower than about 0.4 s, that are closer to the higher vibration modes of the system.

In both the 3D model and the ROM, the bedrock motion is applied to the base of the soil domain, as indicated in Section 3, to carry out a nonlinear, time-domain analysis of the soil-bridge model. The focus is on the longitudinal response of the integral bridge as the one more affected by dynamic soil-structure interaction.[37–39,48] The dynamic perturbation for the coupled soil-bridge models therefore consists of a purely longitudinal seismic motion.

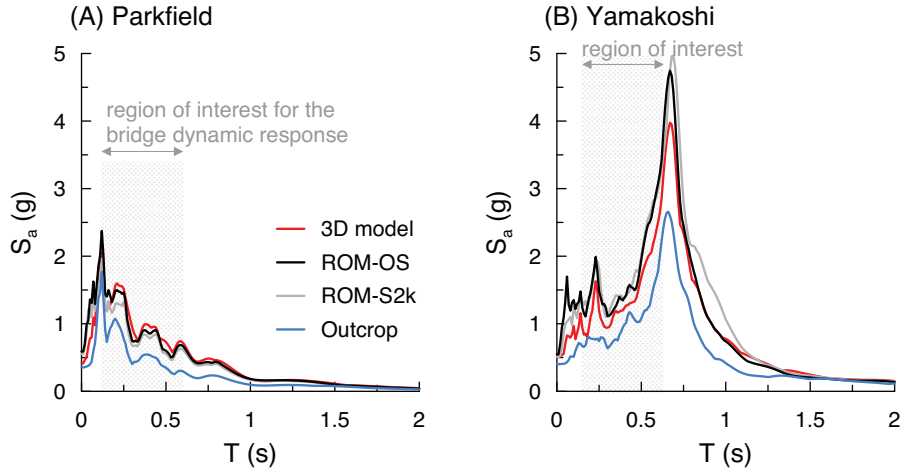

FIGURE 9 Comparison between the 5%-damped elastic response spectra of the motion at the base of the embankments computed through the 3D model, the ROM-OS, the ROM-S2k, and the motion at the outcrop for the selected ground motion scenarios.

4.4 | Site response

As pointed out in Section 4.1, the dynamic response of the bridge is primarily controlled by the soil response. Therefore, it is important to examine the seismic response of the soil-embankment system to gain a first indication of the seismic actions transferred to the structure. To this purpose, Figure 9 depicts the 5%-damped elastic response spectra of the seismic motion computed 'in the free-field' at the base of the embankment (z = 0 m), obtained through the 3D model, the ROM-OS and the ROM-S2K. The figure shows also the outcrop motion used as input for comparison purposes.

As a general comment, the ROM provide a site response similar to that obtained with the reference 3D model, in terms of both frequency content and spectral amplitudes. The ROM-OS is seen to provide a better approximation of the ROM-S2K, as an effect of the improved formulation of the Bouc-Wen model assigned to the soil columns in OpenSees (see Section 3.2). For both the selected ground motion scenarios, amplification occurs up to a period of about 1.3 s. The Yamakoshi record is significantly amplified around its predominant peak, because this signal excites the fundamental mode of the soil domain ($T = 0.62$ s). For this same record, a more limited amplification occurs in the period interval of 0.15–0.3 s, corresponding to the higher modes of the soil-structure system that however produce motion amplitudes still larger than those of the Parkfield record (note the secondary peak at around 0.25 s, close to the period of corresponding fourth and third mode of the full 3D model and ROM, respectively).

4.5 | Bridge response

The dynamic response of the bridge was investigated through dynamic analyses carried out in the time domain, aimed at testing the proposed ROM against the results of the advanced, three-dimensional soil-bridge model. In the following, the seismic performance of the bridge is concisely expressed through the time histories of the bending moment in the two scrutiny points selected for the structural response, namely the deck-abutment connection and the top of the piles. These results are depicted in Figure 10, referring to the left-hand abutment for the deck-abutment contact and to the right-hand one for the piles top section, where the internal forces produced by both ground motions are largest (they would obviously reverse upon sign inversion).

If compared with the results of the full 3D model, the two implementations of the reduced-order modelling provide a satisfactory approximation of the time-evolution of the bending moment in the structure. More in detail, they provide a very good approximation of the maximum bending moment at the deck-abutment contact, whereas they are somewhat less successful in predicting the maximum moment at the piles head.

Table 5 reports numerical values of the peak bending moments at the chosen sections obtained from the three models. The simplified ROMs underestimate systematically the peak bending moments. In most of the cases this underestimate is acceptable, being quite smaller than 10 %. However, for the more severe Yamakoshi record the less refined ROM-S2k model underestimates the bending moments at the piles head by almost 30%. An additional analysis, in which the

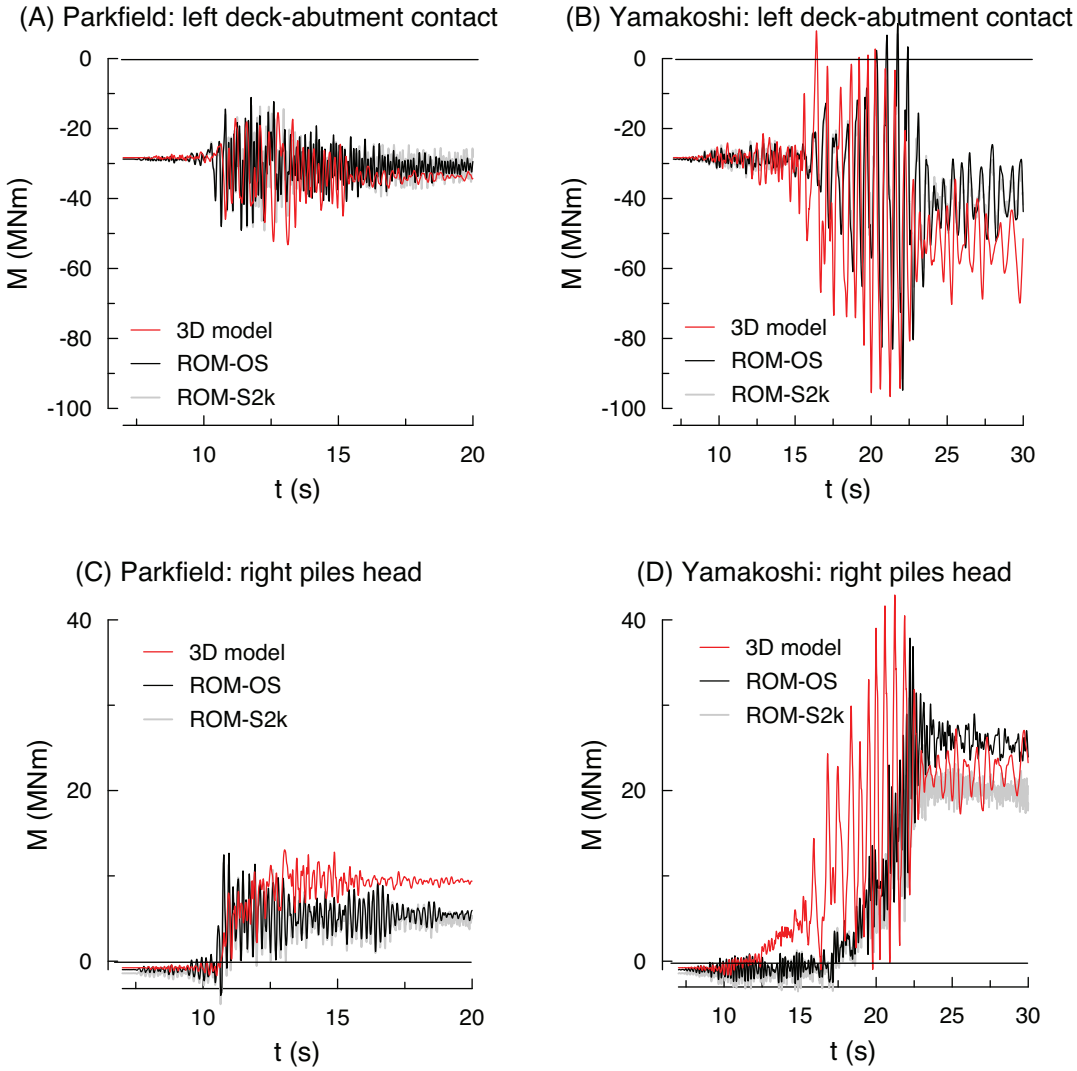

FIGURE 10 Time evolution of the bending moment (A,B) at the left deck-abutment contact and (C,D) at the right piles head, for the two selected seismic scenarios.

TABLE 5 Maximum values of the bending moments obtained from the three models and relative error with respect the 3D model

		3D model	ROM-OS	ROM-S2k		
Motion	**Section**	M_{max} **(MNm)**	M_{max} **(MNm)**	**error (%)**	M_{max} **(MNm)**	**error (%)**
Parkfield	Deck-abutment joint	53.2	49.1	−7.7	49.2	−7.6
	Piles	13.1	12.7	−3.1	11.6	−11
Yamakoshi	Deck-abutment joint	96.6	94.8	−1.9	91.7	−5.1
	Piles	42.9	37.9	−12	30.9	−28

ROM-OS model was re-run replacing the enhanced BWGG model with the same version of the BW available in Sap2000, produced a similar result, confirming that the estimate of the pile moments due to the most severe Yamakoshi record is particularly sensitive to the accuracy of the model used to simulate the response of the soil column.

Significant residual values of the bending moment are obtained at the end of the earthquake, especially for the Yamakoshi scenario, as an effect of important plastic deformations of the soil. In fact, this is the effect of restraining the accumulation of displacements typical of the dynamic response of non-integral bridge abutments[37–39,70,71]: for the latter, under dynamic conditions, the inertial effects in the embankment magnify the abutment response, leading to a cyclic accumulation of displacements associated with the attainment of the active resistance in the soil. The ROM reproduces

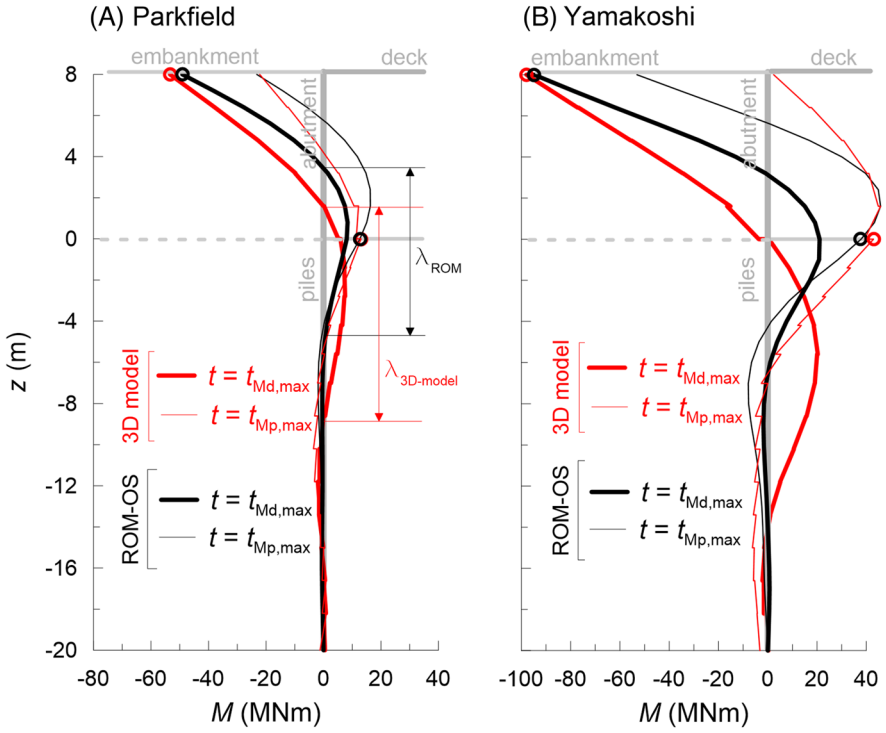

FIGURE 11 Bending moment diagrams in the piles and in the abutment front wall at the time in which the maximum bending moment occurs ($t = t_{\mathrm{Md,max}}$ and $t = t_{\mathrm{Mp,max}}$) for the (A) Parkfield and (B) Yamakoshi seismic motion. Note that the maxima at the two control sections occur at different time instants and on different sides: the maximum pile moments occur on the right abutment and are represented mirrored on the right abutment in the figure. Markers indicate values compared in Table 5.

this accumulation of internal forces, even though the difference of these residual quantities with those from the refined model is larger than for maximum ones. However, it should be considered that previous works showed how the PDMY material used in the 3D model overestimates permanent deformations in the soil, [49,55] and therefore, the discrepancies on the post-earthquake conditions between the two modelling techniques can be partly ascribed to this aspect. Further, the design of the structural members is based on the maximum, instantaneous bending moments, that are reasonably captured by the ROM. The temporal evolution of the longitudinal bending moment at the deck-abutment contact is instead a distinctive feature of the integral deck-abutment connection, which becomes the most stressed component of the bridge. The maximum values of the bending moment at this location are well reproduced by the OpenSees implementation of the ROM, occurring at $t_{Md,max} = 11.39\ s$ and $t_{Md,max} = 22.08\ s$ for the Parkfield and Yamakoshi records, respectively.

Figure 11 compares the profile of the bending moment along the abutment-piles system obtained at two different time instants, relative to the attainment of the maximum moment at the deck-abutment connection ($M_{\mathrm{d,max}}$) and at the piles head ($M_{\mathrm{p,max}}$). Figure 12 shows the corresponding profiles of the horizontal displacement.

While the maximum values at the control sections show a good match, the distributions of the bending moment along the abutment-pile system are not entirely consistent, in that the distance λ between consecutive contraflexure points is somewhat larger in the 3D model than in the ROM (Figure 11A). This same difference is also apparent in the displacement profiles of Figure 12. Since the bending stiffness of the structural elements is the same in the two models, this finding indicates that the description of the soil-structure contact in the ROM (nonlinear longitudinal springs instead of the representation through brick elements used in the 3D model) results in a stiffer response of the soil, and therefore in a smaller structure-soil relative stiffness. Despite this, the good match of the modal response for the two models, together with the similarity of the values computed for the maximum bending moments, suggest that this local discrepancy does not have a substantial influence of the overall response of the system, which is controlled by the response of the free-field soil column and by the properties of the structural elements.

Finally, as a verification of the initial assumption of linear behaviour for the structure, the maximum bending moments, M_{max}, in the critical structural components are compared with the corresponding yield moments, M_{y}. The latter were evaluated in a simplified manner referring to the axial forces in the cross sections of the abutments and of the piles under static conditions (Stage 6 in Figure 3). The resulting yield moments at the top of the abutment and of the pile group are equal to 115 MNm and 39 MNm, respectively. Referring to the results of the 3D model, it follows that the distance from the

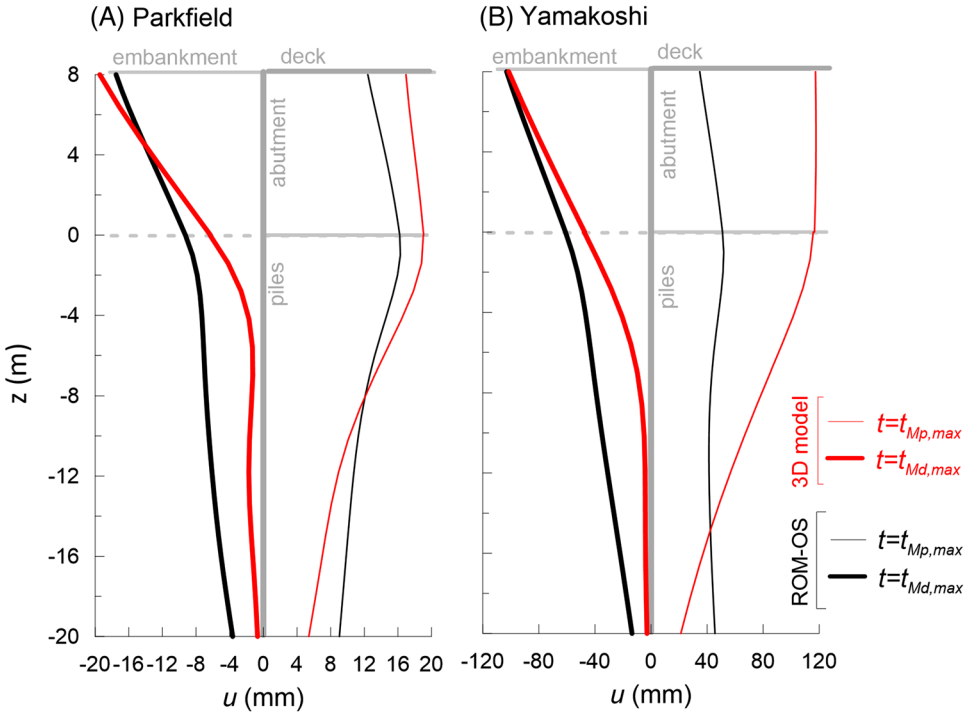

FIGURE 12 Horizontal displacements of the piles and the abutment front wall computed at the time instants corresponding to the maximum bending moment.

yield condition at the deck-abutment contact is equal to M_y / M_{max} = 2.3, 1.2 in the case of the Parkfield and Yamakoshi records, respectively, and at the piles head is M_y / M_{max} = 2.6, 0.9. This means that, while the results are fully consistent with the assumptions for the Parkfield scenario, in the more severe Yamakoshi scenario piles would in fact experience some minor yielding. As it has already been pointed out, inelasticity in the structural members may be easily simulated in the ROM by considering more sophisticated nonlinear constitutive laws for the structural elements.

In light of the discussion above, the predictive capabilities of the ROM can be deemed reasonably good, considering the level of simplification introduced in the numerical modelling of such articulated soil-structure systems. An aspect that has not been pointed out yet concerns the high computational efficiency of the ROM. Each dynamic analysis on the 3D model took about ten days on a multi-core machine using the OpenSees parallel computing through the OpenSeesSP application; by contrast, a dynamic analysis on the ROM can be easily carried out on conventional laptops using the sequential computing of the standard OpenSees application, taking on average less than 1 min per simulation.

5 | CONCLUSION

An integral connection at the deck-abutment contact is an attractive design solution to minimise the maintenance costs of a bridge. For this structural scheme, cyclic thermal effects may be controlled using a compliant abutment, but in turn this design solution has the effect of producing an important coupling between the longitudinal response of the deck and the behaviour of the soil in contact with the abutment. This affects the choice of construction sequence and has remarkable effects on the response of the bridge to longitudinal seismic forces.

Therefore, the design of an integral bridge cannot neglect the interaction of the structure with the foundation soil and with the approach embankment. This soil-structure interaction problem can be tackled at different levels of complexity. Since even small inward displacements of the abutments imply the activation of the active limit state in the approach embankments, soil nonlinearity needs to be included in any realistic interaction model.

This paper compared two different modelling strategies to take into account soil-structure interaction: one is a refined coupled three-dimensional numerical representation of the soil-structure domain, while the other is also coupled, in that it includes explicitly the soil in the analysis model, but it is simplified because it does so by using an assembly of masses and springs. The presence of the soil is described as a combination of a free-field ground response, taken into account through the analysis of a soil column, and the soil-structure interaction, obtained by linking the free-field soil response

to the structural response through uncoupled non-linear independent springs. The simplified model aims at reproducing the sole longitudinal response of a straight non-skew integral abutment bridges and is conceived to carry out non-linear time-domain analyses. Although the case study presented in the paper assumes a linear structural behaviour, structural non-linearity can be easily included through the use of appropriate structural elements if the goal is not design but, rather, the assessment of an existing IAB.

This simplified model has been systematically compared with the higher-order 3D model. Despite the large differences in complexity, the responses provided by the two models, both during the construction stages and under seismic action, were seen to be in a good agreement. The two models showed a comparable modal response, and a similar temporal variation in the internal forces when subjected to two very different seismic motions. Minor discrepancies, related to the instantaneous distribution of the internal forces in the pile-abutment system, appeared to be related to the discontinuous representation of the soil in the simplified model. Nonetheless, provided the more refined implementation of the simplified model is considered, the differences in maximum values of bending moments at the selected control sections were found to be more than acceptable, and certainly so for design purposes, especially in view of the difference in computational effort entailed by the two models.

ACKNOWLEDGEMENTS

This study was funded by the Universita degli Studi di Roma La Sapienza. The opinions and conclusions presented by the authors do not necessarily reflect those of the funding agency. The authors also wish to acknowledge the Texas Advanced Computing Center for the use of the high-performance computing resources of the DesignSafe facility, by which most of the numerical analyses on the advanced, 3D model were carried out.[72] Finally, the authors wish to thank Dr. Fabrizio Noto for fruitful discussion in the initial stage of this work.

DATA AVAILABILITY STATEMENT

The data that support the findings of this study are available from the corresponding author upon reasonable request.

ORCID

Andrea Marchi https://orcid.org/0000-0001-6645-3633
Domenico Gallese https://orcid.org/0000-0002-1202-0995
Davide Noè Gorini https://orcid.org/0000-0001-6673-0071
Paolo Franchin https://orcid.org/0000-0002-1995-0415
Luigi Callisto https://orcid.org/0000-0001-9795-7420

REFERENCES

1. Waldin J, Jennings J, Routledge P. Critically damaged bridges and concepts for earthquake recovery. *NZSEE Conference*. 2012.
2. Wood JH, Earthquake design of bridges with integral abutments. Proceedings of the 6th international conference on earthquake geotechnical engineering, Christchurch, New Zealand. 2015.
3. Maruri R, Petro S. Integral abutments and jointless bridges (IAJB) 2004 survey summary. *FHWA conference*. 2005.
4. Ferretti Torricelli L, Marchiondelli A. The Gatteo integral highway overpass. *Bridge Mainten Safety Manage Life Extens*. 2014. doi:10.1201/b17063-340
5. Dhar S, Kaustubh D. Seismic soil structure interaction for integral abutment bridges: a review. *Trans Infrastruct Geotechnol*. 2019;6(4):249-267.
6. Mahjoubi S, Maleki S. Finite element modelling and seismic behaviour of integral abutment bridges considering soil–structure interaction. *Eur J Environ Civil Eng*. 2020:1-20.
7. Mitoulis SA. Challenges and opportunities for the application of integral abutment bridges in earthquake-prone areas: a review. *Soil Dynamics Earthquake Eng*. 2020;135:106183.
8. White IIH, Pétursson H, Collin P. Integral abutment bridges: the European Way. *ASCE Pract Period Struct Des Constr*. 2010;15:201-208.
9. White H. Wingwall type selection for integral abutment bridges: survey of current practice the United States of America. *Special report 154. Transportation research and development bureau*. New York State Department of Transportation; 2008.
10. Nakamura S, Momijama Y, Hosaka T, Homma K. New technologies of steel/concrete composite bridges. *J Constr Steel Res*. 2002;58:99-130.
11. Akiyama H, Kajikawa Y. Fundamentally structural characteristics of integral bridges. Doctoral dissertation, Graduate School of Natural Science and Technology Kanazawa University, Japan. 2008
12. Connal J. *Integral abutment bridges-Australian and US practice*. 2004. 5th Austroads bridge conference.
13. Caristo A, Barnes J, Mitoulis SA. Numerical modelling of integral abutment bridges under seasonal thermal cycles. *Proc Inst Civil Eng Bridge Eng*. 2018;171(3):179-190. doi:10.1680/jbren.17.00025

14. England GL, Tsang NCM, Bush DI. *Integral bridges: a fundamental approach to the time–temperature loading problem*. 2000. doi:10.1680/ibafattttlp.35416
15. Lehane BM. Lateral soil stiffness adjacent to deep integral bridge abutments. *Géotechnique*. 2011;61(7):593-603. doi:10.1680/geot.9.P.135
16. Muir Wood D, Nash D. Earth pressures on an integral bridge abutment: a numerical case study. *Soils Foundations*. 2000;40(6):23-38. https://doi.org/10.3208/sandf.40.6_23
17. Springman SM, Norrish ARM, Ng CWW. *Cyclic loading of sand behind integral bridge abutments*. Transport Research Laboratory; 1996. TRL Project Report 146.
18. Dicleli M, Eng P, Albhaisi SM. Maximum length of integral bridges supported on steel H-piles driven in sand. *Eng Struct*. 2003;25(12):1491-1504. doi:10.1016/S0141-0296(03)00116-0
19. Dicleli M, Albhaisi SM. Estimation of length limits for integral bridges built on clay. *J Bridge Eng*. 2004;9(6):572-581. doi:10.1061/(ASCE)1084-0702(2004)9:6(572)
20. Wasserman EP, Walker JH. Structural Division: tennessee Department of Transportation for the American Iron and Steel Institute. *Highway Structures Design Handbook*. 1996. Integral abutments for steel bridges. volume 2.
21. BA 42/96. *Design manual for roads and bridges. Highway structures: approval procedures and general design, sect.3. general design, Part 12, the design of integral bridges*. vol. 1. Highways Agency. 1996.
22. BA 42/96 amendment No.1 *Design manual for roads and bridges. Highway structures: approval procedures and general design, sect.3. general design, Part 12, amendment No.1, the design of integral bridges*, vol. 1. Highways Agency. 2003.
23. Burke MP. *Integral and semi-integral bridges*. Wiley-Blackwell; 2009.
24. Werner SD, Beck JL, Levine MB. Seismic response evaluation of Meloland Road overpass using 1979 Imperial Valley earthquake records. *Earthquake Eng Struct Dynamics*. 1987;15(2):249-274. doi:10.1002/eqe.4290150207
25. Wilson JC, Tan BS. Bridge abutments: formulation of simple model for earthquake response analysis. *J Eng Mech*. 1990a;116(8):1828-1837. doi:10.1061/(ASCE)0733-9399(1990)116:8(1828)
26. Wilson JC, Tan BS. Bridge abutments: assessing their influence on earthquake response of Meloland Road overpass. *J Eng Mech*. 1990b;116(8):1838-1856. doi:10.1061/(ASCE)0733-9399(1990)116:8(1838)
27. Goel RK, Chopra AK. Evaluation of bridge abutment capacity and stiffness during earthquakes. *Earthquake Spectra*. 1997;13(1):1-23. doi:10.1193/1.1585929
28. Goel RK. Earthquake characteristics of bridges with integral abutments. *J Struct Eng*. 1997;123(11):1435-1443. doi:10.1061/(ASCE)0733–9445(1997)123:11(1435)
29. McCallen DB, Romstad KM. Dynamic analyses of a skewed short-span, box-girder overpass. *Earthquake Spectra*. 1994;10(4):729-755. doi:10.1193/1.1585795
30. Zhang J, Makris N. Kinematic response functions and dynamic stiffnesses of bridge embankments. *Earthquake Eng Struct Dynamics*. 2002a;31(11):1933-1966.
31. Zhang J, Makris N. Seismic response analysis of highway overcrossings including soil-structure interaction. *Earthquake Eng Struct Dynamics*. 2002b;31(11):1967-1991.
32. Kotsoglou AN, Pantazopoulou SJ. Bridge–embankment interaction under transverse ground excitation. *Earthquake Eng Struct Dynamics*. 2007;36(12):1719-1740. doi:10.1002/eqe.715
33. Kwon OS, Elnashai AS. Seismic analysis of Meloland Road Overcrossing using multiplatform simulation software including SSI. *J Struct Eng*. 2008;134(4):651-660. doi:10.1061/(ASCE)0733-9445(2008)134:4(651)
34. Price T, Eberhard M. Factors contributing to bridge-embankment interaction. *J Struct Eng*. 2005;131(9):1345-1354. doi:10.1061/(ASCE)0733–9445(2005)131:9(1345)
35. Rahmani A, Taiebat M, Finn L, W D. Nonlinear dynamic analysis of Meloland Road Overpass using three-dimensional continuum modeling approach. *Soil Dynamics Earthquake Eng*. 2014;57:121-132. doi:10.1016/j.soildyn.2013.11.004
36. Rahmani A, Taiebat M, Liam Finn WD, Ventura CE. Evaluation of substructuring method for seismic soil-structure interaction analysis of bridges. *Soil Dynamics Earthquake Eng*. 2016;90:112-127. doi:10.1016/j.soildyn.2016.08.013
37. Elgamal, Yan L, Yang Z, Conte JP. Three-dimensional seismic response of Humboldt Bay bridge-foundation-ground system. *J Struct Eng*. 2008;134(7):1165-1176. doi:10.1061/(ASCE)0733-9445(2008)134:7(1165)
38. Gorini DN, Callisto L. A coupled study of soil-abutment-superstructure interaction. *Springer International Publishing*. 2020a:565-574. doi:10.1007/978-3-030-21359-6_60. Geotechnical Research for Land Protection and Development.
39. Gorini DN, Callisto L, Whittle AJ. An inertial macro-element for bridge abutments. *Geotechnique*. 2022;72(3):247-259. doi:10.1680/jgeot.19.P.397
40. Gorini DN, Callisto L, Whittle A. Dominant responses of bridge abutments. *Soil Dynamics Earthquake Eng*. 2021;148:106723. doi:10.1016/j.soildyn.2021.106723
41. Stefanidou SP, Sextos AG, Kotsoglou AN, Lesgidis N, Kappos AJ. Soil structure interaction effects in analysis of seismic fragility of bridges using an intensity-based ground motion selection procedure. *Eng Struct*. 2017;151:366-380. doi:10.1016/j.engstruct.2017.08.033
42. Taskari O, Sextos A. Probabilistic assessment of abutment-embankment stiffness and implications in the predicted performance of short bridges. *J Earthquake Eng*. 2015;19(5):822-846. doi:10.1080/13632469.2015.1009586
43. Greimann LF, Yang P, Wolde-Tinsae AM. Nonlinear analysis of integral abutment bridges. *J Struct Eng*. 1986;112:2263-2280.
44. Faraji S, Ting JM, Crovo DS, Ernst H. Nonlinear analysis of integral bridges: finite-element model. *J Geotech Geoenviron Eng*. 2001;127(5):454-461.

45. Dicleli M, Erhan S. Effect of soil–bridge interaction on the magnitude of internal forces in integral abutment bridge components due to live load effects. *Eng Struct*. 2010;32(1):129-145.
46. Dicleli M, Erhan S. Effect of foundation soil stiffness on the seismic performance of integral bridges. *Struct Eng Int*. 2011;21(2):162-168.
47. Franchin P, Pinto PE, Noto F, A Simplified Nonlinear Dynamic Model for Seismic Analysis of Earth-Retaining Diaphragm-Walls. In *4th International Conference on Earthquake Geotechnical Engineering*. 2007.
48. Franchin P, Pinto PE. Performance-Based Seismic Design of Integral Abutment Bridges. *Bull Earthquake Eng*. 2013;12(2):939-960.
49. Gorini DN. *Soil-structure interaction for bridge abutments: two complementary macro-elements*. PhD thesis, Sapienza University of Rome. Tratto da; 2019. http://hdl.handle.net/11573/1260972
50. Italian Building Code Norme Tecniche per le Costruzioni. D.M. 14.01.2008. Italian Ministry of Infrastructures and Transportation, Rome (in Italian). 2018.
51. Thiagarajan G, Gopalaratnam V, Halmen C, et al. *Bridge approach slabs for Missouri DOT. Looking at alternative and cost efficient approaches*. Missouri Dept. of Transportation; 2010. Rep. No. OR11.009.
52. Dreier D, Burdet O, Muttoni A. Transition slabs of integral abutment bridges. *Struct Eng Int*. 2011;21(2):144-150. doi:10.2749/101686611X12994961034174
53. OptumCE. OptumG2 v. Manual. 2016. https://optumce.com/products/brochure-and-datasheet/
54. McKenna F, Scott MH, Fenves GL. Nonlinear finite-element analysis software architecture using object composition. *J Comput Civil Eng*. 2010. doi:10.1061/(ASCE)CP.1943-5487.0000002
55. Gallese D. *Soil-structure interaction for the seismic design of integral abutment bridges: from advanced numerical modelling to simplified procedures*. PhD thesis, Sapienza University of Rome. 2022. 10.13140/RG.2.2.29620.32642
56. Gallese D, Gorini DN, Callisto L. A nonlinear static analysis for the seismic design of single-span integral abutment bridges. Submitted to Géotechnique. 2022.
57. McGann CR, Arduino P, Mackenzie-Helnwein P. A stabilized single-point finite element formulation for three-dimensional dynamic analysis of saturated soils. *Comput Geotech*. 2015. doi:10.1016/j.compgeo.2015.01.002
58. Yang Z, Elgamal A, Parra E. Computational model for cyclic mobility and associated shear deformation. *J Geotech Geoenviron Eng*. 2003. doi:10.1061/(asce)1090-0241(2003)129:12(1119)
59. Joyner WY, Chen ATF. Calculation of nonlinear ground response in earthquakes. *Bull Seismol Soc Am*. 1975;65(5):1315-1336.
60. McKenna F, Fenves GL. Using the OpenSees interpreter on parallel computers. *Network for Earthquake Engineering Simulations*. 2008. http://opensees.berkeley.edu/OpenSees/parallel/TNParallelProcessing.pdf
61. Marchi A. *Simplified seismic analysis of straight integral frame-abutment bridges.*Doctoral dissertation. Sapienza University of Rome; 2022.
62. SAP2000. Accessed June 2, 2021. https://www.csiamerica.com/products/sap2000
63. CEN. Eurocode 8 — Design of structures for earthquake resistance — Part 2: bridges. *European Committee for Standardization*. Technical Committee 250, Sub-Committee 8, Technical report N1182. 2022.
64. Lancellotta R. Analytical solution of passive earth pressure. *Géotechnique*. 2002;52(8):617-619.
65. Bouc R. A mathematical model for hysteresis. *Acta Acustica United Acustica*. 1971;24(1):16-25.
66. Wen Y-K. Method for random vibration of hysteretic systems. *J Eng Mech Div*. 1976;102(2):249-263.
67. Gerolymos N, Gazetas G. Constitutive model for 1-D cyclic soil behaviour applied to seismic analysis of layered deposits. *Soils Foundations*. 2005;45:147-159.
68. Drosos VA, Gerolymos N, Gazetas G. Constitutive model for soil amplification of ground shaking: parameter calibration, comparisons, validation. *Soil Dynamics Earthquake Eng*. 2012;42:255-274.
69. Ishibashi I, Zhang X. Unified Dynamic Shear Moduli and Damping Ratios of Sand and Clay. *Soils Foundations*. 1993;33(1):182-191.
70. Franchin P, Pinto PE. Analysis of diaphragm-type bridge abutments before and after seismic upgrading. *Proceedings of the 1st us-Italy workshop on seismic design and assessment of bridges*. 2007.
71. Gorini DN, Callisto L. A macro-element approach to analyse bridge abutments accounting for the dynamic behaviour of the superstructure. *Geotechnique*. 2020b;70(8):711-719. doi:10.1680/jgeot.19.ti.012
72. Rathje E, Dawson C, Padgett JE, et al. DesignSafe: a new Cyberinfrastructure for natural hazards engineering. *ASCE Natural Hazards Rev*. 2017. doi:10.1061/(ASCE)NH.1527-6996.0000246
73. Becci B, Nova R. A method for analysis and design of flexible sheetpiles. *Riv Ital Geotec*. 1987;1(87):33-47.

How to cite this article: Marchi A, Gallese D, Gorini DN, Franchin P, Callisto L. On the seismic performance of straight integral abutment bridges: From advanced numerical modelling to a practice-oriented analysis method. *Earthquake Engng Struct Dyn*. 2023;52:164–182. https://doi.org/10.1002/eqe.3755

APPENDIX

Figure A1 provides a graphical description of how the input mechanical and geometrical properties of the soil and structure, as well as the seismic input, are mapped to the model parameters for the OpenSees implementation of the ROM.

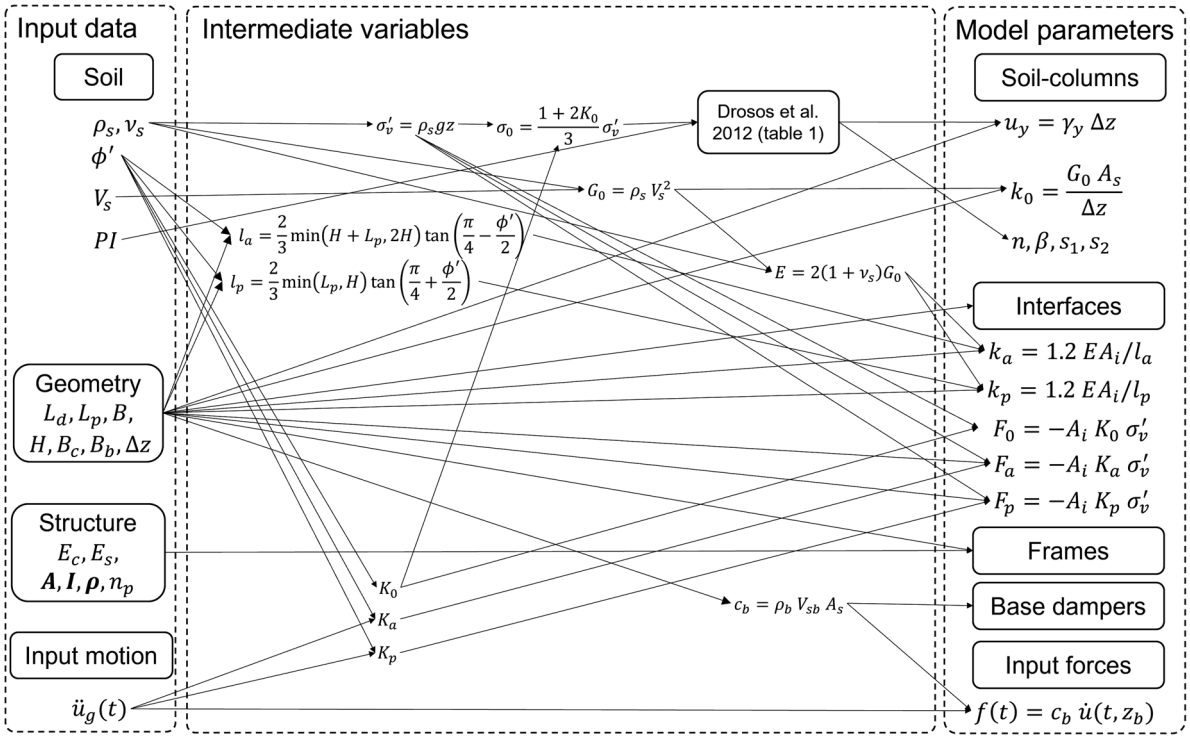

FIGURE A1 Relation between input data and model parameters for the OpenSees implementation of the ROM.

Symbols not defined in the text or in Figure 5 are: the soil Poisson ratio ν_s; the soil vertical stress σ'_v and confinement stress σ'_0; the embankment base and crest width, B_b and B_c, which for the Gatteo case study coincide with the abutment width B; the number of piles n_p; concrete and steel Young moduli E_c and E_s (note that a single symbol is used in the text, because sectional properties for the elastic members are homogenised either to concrete, e.g., for the abutment and piles, or steel, for the deck and only the product EI matters); the mass density ρ_b and shear wave velocity V_{sb} at the model base; the Bouc-Wen parameters β and n; the soil "yield" shear strain γ_y, and the degradation parameters s_1 and s_2, according to Drosos et al.[68] Note that, if the regular Bouc-Wen model is used, rather than the enhanced one in Gerolymos and Gazetas,[67] the same β and n from Drosos et al can be used, but s_1 and s_2 are disregarded and the yield force can be specified as $F_y = k_0 u_y$. Bold symbols denote vectors of area, moment of inertia and weight per unit length of frame members. The reported expressions for the active and passive length entering the interface spring stiffnesses are those from Becci and Nova.[73]